Biomedical Optics EXPRESS

Characterization of eosinophilic esophagitis murine models using optical coherence tomography

Aneesh Alex,[1,2] Mario Noti,[3,4,5] Elia D. Tait Wojno,[3,4,5] David Artis,[3,4,5] and Chao Zhou[1,2,6,*]

[1] *Department of Electrical and Computer Engineering, Lehigh University, Bethlehem, PA-18015, USA*
[2] *Center for Photonics and Nanoelectronics, Lehigh University, Bethlehem, PA-18015, USA*
[3] *Department of Microbiology University of Pennsylvania, Philadelphia, PA 19104, USA*
[4] *Institute for Immunology, Perelman School of Medicine University of Pennsylvania, Philadelphia, PA 19104, USA*
[5] *Department of Pathobiology, School of Veterinary Medicine, University of Pennsylvania, Philadelphia, PA 19104, USA*
[6] *Bioengineering Program, Lehigh University, Bethlehem, PA-18015, USA*
[*] *chaozhou@lehigh.edu*

Abstract: Pre-clinical studies using murine models are critical for understanding the pathophysiological mechanisms underlying immune-mediated disorders such as Eosinophilic esophagitis (EoE). In this study, an optical coherence tomography (OCT) system capable of providing three-dimensional images with axial and transverse resolutions of 5 µm and 10 µm, respectively, was utilized to obtain esophageal images from a murine model of EoE-like disease *ex vivo*. Structural changes in the esophagus of wild-type ($Tslpr^{+/+}$) and mutant ($Tslpr^{-/-}$) mice with EoE-like disease were quantitatively evaluated and food impaction sites in the esophagus of diseased mice were monitored using OCT. Here, the capability of OCT as a label-free imaging tool devoid of tissue-processing artifacts to effectively characterize murine EoE-like disease models has been demonstrated.

OCIS codes: (110.4500) Optical coherence tomography; (110.6880) Three-dimensional image acquisition; (170.0110) Imaging systems; (170.2680) Gastrointestinal; (170.3880) Medical and biological imaging; (170.6935) Tissue characterization.

References and links

1. R. J. Noel, P. E. Putnam, and M. E. Rothenberg, "Eosinophilic esophagitis," N. Engl. J. Med. **351**(9), 940–941 (2004).
2. A. Straumann, H.-P. Spichtin, L. Grize, K. A. Bucher, C. Beglinger, and H.-U. Simon, "Natural history of primary eosinophilic esophagitis: a follow-up of 30 adult patients for up to 11.5 years," Gastroenterology **125**(6), 1660–1669 (2003).
3. H. Korsapati, A. Babaei, V. Bhargava, R. Dohil, A. Quin, and R. K. Mittal, "Dysfunction of the longitudinal muscles of the oesophagus in eosinophilic oesophagitis," Gut **58**(8), 1056–1062 (2009).
4. C. Blanchard and M. E. Rothenberg, "Basic pathogenesis of eosinophilic esophagitis," Gastrointest. Endosc. Clin. N. Am. **18**(1), 133–143 (2008).
5. M. E. Rothenberg, "Biology and treatment of eosinophilic esophagitis," Gastroenterology **137**(4), 1238–1249 (2009).
6. C. Blanchard, E. M. Stucke, K. Burwinkel, J. M. Caldwell, M. H. Collins, A. Ahrens, B. K. Buckmeier, S. C. Jameson, A. Greenberg, A. Kaul, J. P. Franciosi, J. P. Kushner, L. J. Martin, P. E. Putnam, J. P. Abonia, S. I. Wells, and M. E. Rothenberg, "Coordinate interaction between IL-13 and epithelial differentiation cluster genes in eosinophilic esophagitis," J. Immunol. **184**, 4033–4041 (2010).
7. M. E. Rothenberg, J. M. Spergel, J. D. Sherrill, K. Annaiah, L. J. Martin, A. Cianferoni, L. Gober, C. Kim, J. Glessner, E. Frackelton, K. Thomas, C. Blanchard, C. Liacouras, R. Verma, S. Aceves, M. H. Collins, T. Brown-Whitehorn, P. E. Putnam, J. P. Franciosi, R. M. Chiavacci, S. F. A. Grant, J. P. Abonia, P. M. A. Sleiman, and H. Hakonarson, "Common variants at 5q22 associate with pediatric eosinophilic esophagitis," Nat. Genet. **42**(4), 289–291 (2010).
8. M. S. Levine, P. Ramchandani, and S. E. Rubesin, *Practical Fluoroscopy of the GI and GU Tracts* (Cambridge University, 2012), p. 235.
9. J. Stoker, *MRI of the Gastrointestinal Tract* (Springer, 2010), p. 353.

#201290 - $15.00 USD Received 14 Nov 2013; revised 17 Jan 2014; accepted 18 Jan 2014; published 27 Jan 2014

10. E. M. Godfrey, S. M. Rushbrook, and N. R. Carrol, "Endoscopic ultrasound: a review of current diagnostic and therapeutic applications," Postgrad. Med. J. **86**(1016), 346–353 (2010).
11. M. W. Shahid and M. B. Wallace, "Endoscopic imaging for the detection of esophageal dysplasia and carcinoma," Gastrointest. Endosc. Clin. N. Am. **20**, 11–24 (2010).
12. J. B. Frøkjaer, A. M. Drewes, and H. Gregersen, "Imaging of the gastrointestinal tract-novel technologies," World J. Gastroenterol. **15**(2), 160–168 (2009).
13. M. Goetz, "Confocal laser endomicroscopy: Applications in clinical and translational science-A comprehensive review," ISRN Pathol. **2012**, 1–13 (2012).
14. A. M. Boeriu, D. E. Dobru, and S. Mocan, "Magnifying endoscopy and chromoendoscopy of the upper gastrointestinal tract," J. Gastrointestin. Liver Dis. **18**(1), 109–113 (2009).
15. K. Yao, Y. Takaki, T. Matsui, A. Iwashita, G. K. Anagnostopoulos, P. Kaye, and K. Ragunath, "Clinical application of magnification endoscopy and narrow-band imaging in the upper gastrointestinal tract: new imaging techniques for detecting and characterizing gastrointestinal neoplasia," Gastrointest. Endosc. Clin. N. Am. **18**, 415–433 (2008).
16. G. J. Tearney, M. E. Brezinski, B. E. Bouma, S. A. Boppart, C. Pitris, J. F. Southern, and J. G. Fujimoto, "In vivo endoscopic optical biopsy with optical coherence tomography," Science **276**(5321), 2037–2039 (1997).
17. B. E. Bouma, G. J. Tearney, C. C. Compton, and N. S. Nishioka, "High-resolution imaging of the human esophagus and stomach in vivo using optical coherence tomography," Gastrointest. Endosc. **51**(4), 467–474 (2000).
18. X. D. Li, S. A. Boppart, J. Van Dam, H. Mashimo, M. Mutinga, W. Drexler, M. Klein, C. Pitris, M. L. Krinsky, M. E. Brezinski, and J. G. Fujimoto, "Optical coherence tomography: advanced technology for the endoscopic imaging of Barrett's esophagus," Endoscopy **32**(12), 921–930 (2000).
19. J. G. Fujimoto, "Optical coherence tomography for ultrahigh resolution in vivo imaging," Nat. Biotechnol. **21**(11), 1361–1367 (2003).
20. Y. Chen, A. D. Aguirre, P. L. Hsiung, S. Desai, P. R. Herz, M. Pedrosa, Q. Huang, M. Figueiredo, S. W. Huang, A. Koski, J. M. Schmitt, J. G. Fujimoto, and H. Mashimo, "Ultrahigh resolution optical coherence tomography of Barrett's esophagus: preliminary descriptive clinical study correlating images with histology," Endoscopy **39**(7), 599–605 (2007).
21. B. J. Vakoc, M. Shishko, S. H. Yun, W.-Y. Oh, M. J. Suter, A. E. Desjardins, J. A. Evans, N. S. Nishioka, G. J. Tearney, and B. E. Bouma, "Comprehensive esophageal microscopy by using optical frequency-domain imaging (with video)," Gastrointest. Endosc. **65**(6), 898–905 (2007).
22. M. J. Suter, B. J. Vakoc, P. S. Yachimski, M. Shishkov, G. Y. Lauwers, M. Mino-Kenudson, B. E. Bouma, N. S. Nishioka, and G. J. Tearney, "Comprehensive microscopy of the esophagus in human patients with optical frequency domain imaging," Gastrointest. Endosc. **68**(4), 745–753 (2008).
23. D. C. Adler, C. Zhou, T. H. Tsai, H. C. Lee, L. Becker, J. M. Schmitt, Q. Huang, J. G. Fujimoto, and H. Mashimo, "Three-dimensional optical coherence tomography of Barrett's esophagus and buried glands beneath neosquamous epithelium following radiofrequency ablation," Endoscopy **41**(9), 773–776 (2009).
24. C. Zhou, T.-H. Tsai, H.-C. Lee, T. Kirtane, M. Figueiredo, Y. K. Tao, O. O. Ahsen, D. C. Adler, J. M. Schmitt, Q. Huang, J. G. Fujimoto, and H. Mashimo, "Characterization of buried glands before and after radiofrequency ablation by using 3-dimensional optical coherence tomography (with videos)," Gastrointest. Endosc. **76**(1), 32–40 (2012).
25. T.-H. Tsai, C. Zhou, Y. K. Tao, H.-C. Lee, O. O. Ahsen, M. Figueiredo, T. Kirtane, D. C. Adler, J. M. Schmitt, Q. Huang, J. G. Fujimoto, and H. Mashimo, "Structural markers observed with endoscopic 3-dimensional optical coherence tomography correlating with Barrett's esophagus radiofrequency ablation treatment response (with videos)," Gastrointest. Endosc. **76**(6), 1104–1112 (2012).
26. H. Neumann and K. Mönkemüller, "Endoscopic characterization of eosinophilic esophagitis," Video Journal and Encyclopedia of GI Endoscopy **1**, 23–24 (2013).
27. M. J. Gora, J. S. Sauk, R. W. Carruth, K. A. Gallagher, M. J. Suter, N. S. Nishioka, L. E. Kava, M. Rosenberg, B. E. Bouma, and G. J. Tearney, "Tethered capsule endomicroscopy enables less invasive imaging of gastrointestinal tract microstructure," Nat. Med. **19**(2), 238–240 (2013).
28. M. H. Collins, "Histopathologic features of eosinophilic esophagitis," Gastrointest. Endosc. Clin. N. Am. **18**, 59–71 (2008).
29. E. S. Dellon, "Eosinophilic esophagitis: diagnostic tests and criteria," Curr. Opin. Gastroenterol. **28**(4), 382–388 (2012).
30. L. O. Diniz, P. E. Putnum, and A. J. Towbin, "Fluoroscopic findings in pediatric eosinophilic esophagitis," Pediatr. Radiol. **42**(6), 721–727 (2012).
31. G. T. Furuta, C. A. Liacouras, M. H. Collins, S. K. Gupta, C. Justinich, P. E. Putnam, P. Bonis, E. Hassall, A. Straumann, and M. E. Rothenberg; First International Gastrointestinal Eosinophil Research Symposium (FIGERS) Subcommittees, "Eosinophilic esophagitis in children and adults: a systematic review and consensus recommendations for diagnosis and treatment," Gastroenterology **133**(4), 1342–1363 (2007).
32. N. Gonsalves, M. Policarpio-Nicolas, Q. Zhang, M. S. Rao, and I. Hirano, "Histopathologic variability and endoscopic correlates in adults with eosinophilic esophagitis," Gastrointest. Endosc. **64**(3), 313–319 (2006).
33. A. Shah, A. F. Kagalwalla, N. Gonsalves, H. Melin-Aldana, B. U. K. Li, and I. Hirano, "Histopathologic variability in children with eosinophilic esophagitis," Am. J. Gastroenterol. **104**(3), 716–721 (2009).
34. C. A. Dinarello, "Immunological and inflammatory functions of the Interleukin-1 family," Annu. Rev. Immunol. **27**(1), 519–550 (2009).

#201290 - $15.00 USD Received 14 Nov 2013; revised 17 Jan 2014; accepted 18 Jan 2014; published 27 Jan 2014

35. V. Aidinis, C. Chandras, M. Manoloukos, A. Thanassopoulou, K. Kranidioti, M. Armaka, E. Douni, D. L. Kontoyiannis, M. Zouberakis, and G. Kollias; Mugen NoE consortium, "MUGEN mouse database; Animal models of human immunological diseases," Nucleic Acids Res. **36**(Database issue), D1048–D1054 (2007).
36. M. Saleh and G. Trinchieri, "Innate immune mechanisms of colitis and colitis-associated colorectal cancer," Nat. Rev. Immunol. **11**(1), 9–20 (2010).
37. D. J. Mulder and C. J. Justinich, "B cells, IgE and mechanisms of type I hypersensitivity in eosinophilic oesophagitis," Gut **59**(1), 6–7 (2010).
38. J. P. Abonia and M. E. Rothenberg, "Eosinophilic esophagitis: rapidly advancing insights," Annu. Rev. Med. **63**(1), 421–434 (2012).
39. J. D. Sherrill, P.-S. Gao, E. M. Stucke, C. Blanchard, M. H. Collins, P. E. Putnam, J. P. Franciosi, J. P. Kushner, J. P. Abonia, A. H. Assa'ad, M. B. Kovacic, J. M. Biagini Myers, B. S. Bochner, H. He, G. K. Hershey, L. J. Martin, and M. E. Rothenberg, "Variants of thymic stromal lymphopoietin and its receptor associate with eosinophilic esophagitis," J. Allergy Clin. Immunol. **126**, 160–165 (2010).
40. M. Noti, E. D. T. Wojno, B. S. Kim, M. C. Siracusa, P. R. Giacomin, M. G. Nair, A. J. Benitez, K. R. Ruymann, A. B. Muir, D. A. Hill, K. R. Chikwava, A. E. Moghaddam, Q. J. Sattentau, A. Alex, C. Zhou, J. H. Yearley, P. Menard-Katcher, M. Kubo, K. Obata-Ninomiya, H. Karasuyama, M. R. Comeau, T. Brown-Whitehorn, R. de Waal Malefyt, P. M. Sleiman, H. Hakonarson, A. Cianferoni, G. W. Falk, M.-L. Wang, J. M. Spergel, and D. Artis, "Thymic stromal lymphopoietin-elicited basophil responses promote eosinophilic esophagitis," Nat. Med. **19**(8), 1005–1013 (2013).
41. C. W. DeBrosse, J. P. Franciosi, E. C. King, B. K. B. Butz, A. B. Greenberg, M. H. Collins, J. P. Abonia, A. Assa'ad, P. E. Putnam, and M. E. Rothenberg, "Long-term outcomes in pediatric-onset esophageal eosinophilia," J. Allergy Clin. Immunol. **128**(1), 132–138 (2011).
42. B. Bhattacharya, J. Carlsten, E. Sabo, S. Kethu, P. Meitner, R. Tavares, S. Jakate, S. Mangray, B. Aswad, and M. B. Resnick, "Increased expression of eotaxin-3 distinguishes between eosinophilic esophagitis and gastroesophageal reflux disease," Hum. Pathol. **38**(12), 1744–1753 (2007).
43. K. S. Hsu Blatman, N. Gonsalves, I. Hirano, and P. J. Bryce, "Expression of mast cell-associated genes is upregulated in adult eosinophilic esophagitis and responds to steroid or dietary therapy," J. Allergy Clin. Immunol. **127**, 1307–1308 (2011).
44. E. Rubinstein, J. Y. Cho, P. Rosenthal, J. Chao, M. Miller, A. Pham, S. S. Aceves, A. Varki, and D. H. Broide, "Siglec-F inhibition reduces esophageal eosinophilia and angiogenesis in a mouse model of eosinophilic esophagitis," J. Pediatr. Gastroenterol. Nutr. **53**(4), 409–416 (2011).
45. J. Kong, M. A. Crissey, S. Funakoshi, J. L. Kreindler, and J. P. Lynch, "Ectopic Cdx2 Expression in Murine Esophagus Models an Intermediate Stage in the Emergence of Barrett's Esophagus," PLoS ONE **6**(4), e18280 (2011).
46. S. Roth, P. Franken, K. Monkhorst, J. Kong a San, and R. Fodde, "Generation and characterization of an inducible transgenic model for studying mouse esophageal biology," BMC Dev. Biol. **12**(1), 18 (2012).
47. D. Huang, E. A. Swanson, C. P. Lin, J. S. Schuman, W. G. Stinson, W. Chang, M. R. Hee, T. Flotte, K. Gregory, C. A. Puliafito, and J. G. Fujimoto, "Optical coherence tomography," Science **254**(5035), 1178–1181 (1991).
48. A. F. Fercher, C. K. Hitzenberger, G. Kamp, and S. Y. El-Zaiat, "Measurement of intraocular distances by backscattering spectral interferometry," Opt. Commun. **117**(1-2), 43–48 (1995).
49. W. Drexler and J. G. Fujimoto, *Optical Coherence Tomography: Technology and Applications* (Springer, 2008), p. 1346.
50. L. P. Hariri, A. R. Tumlinson, N. H. Wade, D. G. Besselsen, U. Utzinger, E. W. Gerner, and J. K. Barton, "Ex vivo optical coherence tomography and laser-induced fluorescence spectroscopy imaging of murine gastrointestinal tract," Comp. Med. **57**(2), 175–185 (2007).
51. A. M. Winkler, P. F. S. Rice, R. A. Drezek, and J. K. Barton, "Quantitative tool for rapid disease mapping using optical coherence tomography images of azoxymethane-treated mouse colon," J. Biomed. Opt. **15**(4), 041512 (2010).
52. N. Iftimia, A. K. Iyer, D. X. Hammer, N. Lue, M. Mujat, M. Pitman, R. D. Ferguson, and M. Amiji, "Fluorescence-guided optical coherence tomography imaging for colon cancer screening: a preliminary mouse study," Biomed. Opt. Express **3**(1), 178–191 (2012).
53. K. L. Corwin, N. R. Newbury, J. M. Dudley, S. Coen, S. A. Diddams, K. Weber, and R. S. Windeler, "Fundamental Noise Limitations to Supercontinuum Generation in Microstructure Fiber," Phys. Rev. Lett. **90**(11), 113904 (2003).
54. J. M. Spergel, T. F. Brown-Whitehorn, J. L. Beausoleil, J. Franciosi, M. Shuker, R. Verma, and C. A. Liacouras, "14 years of eosinophilic esophagitis: clinical features and prognosis," J. Pediatr. Gastroenterol. Nutr. **48**(1), 30–36 (2009).
55. J. A. Lieberman and M. Chehade, "Eosinophilic esophagitis: diagnosis and management," Immunol. Allergy Clin. North Am. **32**(1), 67–81 (2012).
56. E. S. Dellon, "Diagnosis and management of eosinophilic esophagitis," Clin. Gastroenterol. Hepatol. **10**(10), 1066–1078 (2012).
57. C. Zhou, T. Kirtane, T.-H. Tsai, H.-C. Lee, D. C. Adler, J. M. Schmitt, Q. Huang, J. G. Fujimoto, and H. Mashimo, "Cervical inlet patch-optical coherence tomography imaging and clinical significance," World J. Gastroenterol. **18**(20), 2502–2510 (2012).
58. E. S. Dellon, A. Aderoju, J. T. Woosley, R. S. Sandler, and N. J. Shaheen, "Variability in diagnostic criteria for eosinophilic esophagitis: a systematic review," Am. J. Gastroenterol. **102**(10), 2300–2313 (2007).
59. A. R. Tumlinson, L. P. Hariri, U. Utzinger, and J. K. Barton, "Miniature endoscope for simultaneous optical coherence tomography and laser-induced fluorescence measurement," Appl. Opt. **43**(1), 113–121 (2004).

#201290 - $15.00 USD Received 14 Nov 2013; revised 17 Jan 2014; accepted 18 Jan 2014; published 27 Jan 2014

60. A. M. Winkler, P. F. S. Rice, J. Weichsel, J. M. Watson, M. V. Backer, J. M. Backer, and J. K. Barton, "In vivo, dual-modality OCT/LIF imaging using a novel VEGF receptor-targeted NIR fluorescent probe in the AOM-treated mouse model," Mol. Imaging Biol. **13**(6), 1173–1182 (2011).
61. H. G. Bezerra, M. A. Costa, G. Guagliumi, A. M. Rollins, and D. I. Simon, "Intracoronary optical coherence tomography: A comprehensive review clinical and research applications," JACC Cardiovasc. Interv. **2**(11), 1035–1046 (2009).
62. M. C. Santos, T. Lin, and P. Barlis, "In-stent restenosis associated with stent malapposition: seven year optical coherence tomography findings," Int. J. Cardiol. **147**(1), 149–151 (2011).
63. S. Moon, Z. Piao, C.-S. Kim, and Z. Chen, "Lens-free endoscopy probe for optical coherence tomography," Opt. Lett. **38**(12), 2014–2016 (2013).
64. J. Sauk, E. Coron, L. Kava, M. Suter, M. Gora, K. Gallagher, M. Rosenberg, A. Ananthakrishnan, N. Nishioka, G. Lauwers, K. Woods, W. Brugge, D. Forcione, B. E. Bouma, and G. Tearney, "Interobserver agreement for the detection of Barrett's esophagus with optical frequency domain imaging," Dig. Dis. Sci. **58**(8), 2261–2265 (2013).
65. W. Hatta, K. Uno, T. Koike, S. Yokosawa, K. Iijima, A. Imatani, and T. Shimosegawa, "Optical coherence tomography for the staging of tumor infiltration in superficial esophageal squamous cell carcinoma," Gastrointest. Endosc. **71**(6), 899–906 (2010).

1. Introduction

Eosinophilic esophagitis (EoE) is an inflammatory disease of the esophagus characterized by eosinophilic infiltration of the esophageal squamous epithelium [1]. EoE-associated symptoms include feeding difficulties, failure to thrive, epigastric and chest pain, dysphagia and food impactions. Symptoms such as food impaction and dysphagia can be caused by structural esophageal alterations or selective dysfunction of longitudinal muscle contraction during peristalsis [2, 3]. Recently, pre-clinical and clinical studies investigating the signaling pathways and identification of candidate genes involved in the pathogenesis of EoE has been an active area of research [4–7].

In the clinic, imaging techniques such as X-ray fluoroscopy, magnetic resonance imaging (MRI), endoscopic ultrasound (EUS) or high-definition white light endoscopy (hWLE) are typically used to evaluate morphological abnormalities, followed by biopsy for diagnosing upper gastrointestinal (GI) disorders [8–12]. Multiple optical imaging techniques such as confocal laser endomicroscopy (CLE) [13], chromoendoscopy [14], narrow band imaging [15] and optical coherence tomography (OCT) [16–25] have been used in conjunction with hWLE for detecting GI diseases. Recently, an endoscopic study using hWLE and CLE has shown promise in providing more detailed diagnosis of EoE-associated histological changes *in vivo* [26]. In another recent study, a tethered optomechanical pill that was capable of capturing three-dimensional (3D) micromorphologic images using OCT, suitable for diagnostic applications in the upper GI tract, was demonstrated [27]. *In vivo* non-invasive imaging techniques such as CLE and OCT allow visualization of epithelial surface and sub-surface features with micron-scale resolution. Hence, these techniques can be a useful adjunct to endoscopy to improve the diagnostic accuracy in GI diseases and to avoid unnecessary endoscopic biopsies.

Currently, clinical diagnosis of EoE is based on three criteria: clinical symptoms of esophageal dysfunction; an esophageal biopsy with a maximum eosinophil count ≥ 15 eosinophils per high-power microscopy field, with few exceptions and exclusion of other possible causes of esophageal eosinophilia [28]. However, differential diagnosis of EoE remains challenging because no single symptom, endoscopic finding or histopathologic feature is a definitive indicator of EoE [29]. In a recent study using fluoroscopy in pediatric EoE patients, the esophagus in nearly half of the patients appeared normal in fluoroscopic images [30]. Because of the broad variations in endoscopic appearance and the poor understanding of the pathophysiological mechanisms that contribute to the development of esophageal dysfunction in the context of EoE, current guidelines recommend that biopsies should be taken from multiple locations of every patient suspected of suffering from EoE [31]. In addition to being a time-consuming and expensive procedure, endoscopic biopsies are prone to sampling errors and possess minor risks, particularly in pediatric patients [32, 33]. Hence, there is an urgent need to apprehend the fundamental processes involved in EoE pathogenesis and to improve the efficacy of current EoE diagnostic procedures.

#201290 - $15.00 USD Received 14 Nov 2013; revised 17 Jan 2014; accepted 18 Jan 2014; published 27 Jan 2014

To better understand the complex mechanisms regulating the immune system and its pathological processes, it is important to generate experimental animal models that mimic human disorders. In pre-clinical studies, mouse models are used for investigating immune-mediated disorders, due to their similarities with human immunological processes [34] and the accessibility of transgenic mouse strains, allowing for studies that target specific functional pathways [35, 36]. Immunological mechanisms associated with EoE pathogenesis have been linked to various immune cell types including eosinophils, mast cells and lymphocytes, and cytokines [37, 38]. A gain-of-function polymorphism in the gene that encodes the predominantly epithelial cell-derived cytokine, thymic stromal lymphopoietin (TSLP), has been associated with the development of EoE [7, 39]. In a recent study, a murine model of EoE-like disease that is associated with enhanced TSLP production was used to investigate the role of TSLP in the development of EoE [40]. When challenged repeatedly with a model food antigen, ovalbumin (OVA), mice exhibited immunological and pathophysiological changes in esophageal tissues and signs of esophageal dysfunction, similar to those observed in human EoE patients [41–43].

Further important insights into the functional pathways involved in EoE pathogenesis can be obtained by effectively monitoring and characterizing the physiological changes in the esophagus of murine EoE-like disease models. Currently, immunohistochemistry, fluorescence microscopy and histopathology are the methods of choice for characterizing mouse models of various esophageal disorders [44–46]. These techniques can be used to visualize and quantify cell types, nature of pathology and gene expression in target tissues *in vitro*. However, there is a lack of non-invasive label-free experimental tools capable of detecting structural and pathophysiological changes in the esophagus of mouse models *in vivo*. OCT is one of the promising non-invasive *in vivo* optical imaging modalities capable of providing 3D micro-structural information in real-time with micron-scale resolutions and 1 - 2 mm penetration depth in biological tissues [47–49]. OCT gains its structural contrast from the intrinsic scattering properties of the specimen, and does not require the specimen to be fixed or stained. In previous studies, OCT has demonstrated its capability to clearly demarcate different layers of the mouse GI tract [50–52]. In this study, micromorphological features visible in the esophagus of mice with EoE-like disease were investigated using OCT *ex vivo*. Thickness of different esophageal layers obtained from the OCT images of control and mutant mouse strains were compared, and effective diagnostic indicators of murine EoE-like disease were determined.

2. Methods

2.1 OCT system

A spectral domain OCT system using a portion of the near infrared spectrum from a supercontinuum source (SC-400-4, Fianium Ltd., UK), with a center wavelength of ~1300 nm and a bandwidth of ~200 nm was utilized for obtaining esophagus images *ex vivo*. The OCT system was capable of providing axial and transverse resolutions of ~5 μm (in tissue) and ~10 μm, respectively. The system was designed as a Michelson interferometer, in which the light returning from the reference and sample arms was detected using a spectrometer consisting of a 1145 lpmm transmission grating (Wasatch Photonics, Logan, UT, USA) and a 1024-pixel line scan camera (SUI Goodrich, Princeton, NJ, USA). The A-scan rate of the system was 47 kHz. The sensitivity of the OCT system was determined as ~92 dB close to the zero delay position with ~12 mW incident on the sample, and the 6 dB sensitivity roll off depth was ~1.2 mm. Shot-noise limited sensitivity was not achieved owing to the high relative intensity noise from the supercontinuum light source [53]. However, the dynamic range offered by the OCT system was sufficient to quantify the thickness of various esophageal sub-layers.

2.2 Murine EoE-like disease model

In order to determine the role of the TSLP pathway in EoE pathogenesis, wild-type (WT) BALB/c mice ($Tslpr^{+/+}$ mice) and mice deficient in the TSLP receptor ($Tslpr^{-/-}$ mice) were

#201290 - $15.00 USD Received 14 Nov 2013; revised 17 Jan 2014; accepted 18 Jan 2014; published 27 Jan 2014

used in this study. All mice were provided by Amgen Inc. (California, USA) through Charles River Laboratories Inc. (Massachusetts, USA). Mice at 8–12 weeks of age were used for OCT imaging, and all experiments used age- and gender-matched controls. Animals were bred and housed in specific pathogen–free conditions at the University of Pennsylvania. To induce murine EoE-like disease, mice were treated daily for 14 days on the ears with 2 nmol of the vitamin D analog, MC903 (Tocris Bioscience, Bristol, UK) in 20 μL of 100% ethanol (EtOH) in the presence of 100 μg OVA. As a vehicle control, the same volume of EtOH and OVA was applied. All mice groups were challenged intragastrically (IG) with 50 mg OVA on days 14, 17.5, 18, 20, 22, 24 and 26, and were euthanized on day 27. After the first IG OVA challenge, mice were given continuous access to water containing 1.5 g L^{-1} OVA. While *Tslpr*$^{+/+}$ mice developed EoE-like disease following epicutaneous sensitization and repeated challenge with OVA, *Tslpr*$^{-/-}$ mice did not exhibit symptoms of EoE-like disease. The mice group classification and sample size in each group is given in Table 1.

Table 1. Mice group classification and sample size in each group

	***Tslpr*$^{+/+}$**	***Tslpr*$^{-/-}$**
Ethanol + OVA	*Tslpr*$^{+/+}$ control (n = 6)	*Tslpr*$^{-/-}$ control (n = 4)
MC903 + OVA	*Tslpr*$^{+/+}$ treatment (n = 9)	*Tslpr*$^{-/-}$ treatment (n = 6)

To assess food impaction in the esophagus, mice exposed to prolonged esophageal inflammation were fasted for at least 30 min and up to 2 h. Mice were then euthanized, and their esophagi were examined for the presence of impacted food prior to OCT imaging. A licensed veterinarian provided care to any animals requiring medical attention. All experiments were performed under protocols approved by the University of Pennsylvania Institutional Animal Care and Use Committee (IACUC) and in accordance with the guidelines of the IACUC of the University of Pennsylvania.

2.3 Sample preparation and imaging protocol

Prior to OCT imaging, the esophagus was removed from the mouse, and a plastic tube with an outer diameter of 0.75 mm was inserted into the esophagus. This enabled the esophageal lumen surface to be clearly differentiated in the OCT cross-sections. In order to extract esophageal layer thickness accurately with minimal distortion, esophageal specimens were illuminated with the OCT imaging beam from its periphery. The esophagus was immersed in saline solution to keep the sample hydrated and to reduce the bright surface reflection. 3D OCT images were obtained from different locations along the esophagus, with each volume covering 3 x 1.5 x 1.5 mm^3 (1536 x 512 x 1024 voxels). After OCT imaging, the esophagus was fixed in 4% paraformaldehyde and paraffin-embedded. 5 μm sections of esophageal tissue were cut and subsequently stained with hematoxylin and eosin (H & E) for histopathology.

2.4 OCT image analysis

From each specimen, OCT volumetric images were obtained from anterior, middle and posterior regions [Fig. 1(A)]. As the layered arrangement and thickness of different layers showed significant variations in the anterior and posterior regions of the esophagus, only the thickness values obtained from the middle regions were used for analyses [Figs. 1(C) and 1(D)]. Thickness values of different layers of the esophagus were measured from the cross-sectional OCT images every 200 μm within each 3D OCT data set. The layer thickness values estimated from food impaction sites were excluded from analysis. Average thickness values for different layers were calculated from each specimen and statistical comparison of layer thickness values from different mice groups was performed using Student's t-test. Results were considered significantly different at $p \leq 0.05$.

#201290 - $15.00 USD Received 14 Nov 2013; revised 17 Jan 2014; accepted 18 Jan 2014; published 27 Jan 2014

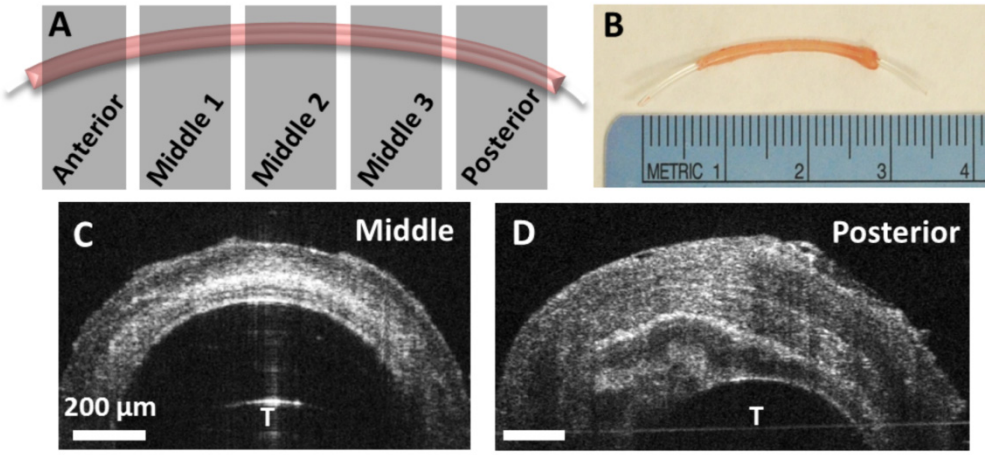

Fig. 1. OCT imaging protocol. A) OCT volumetric data sets (3x1.5x1.5 mm^3) were obtained from five locations along the length of the esophagus. B) Photograph of isolated esophagus with plastic tube inserted. Representative OCT cross-sections from middle (C) and posterior (D) regions of the esophagus showing variations in morphology; T denotes the location of plastic tube.

3. Results

3.1 OCT images of normal esophagus

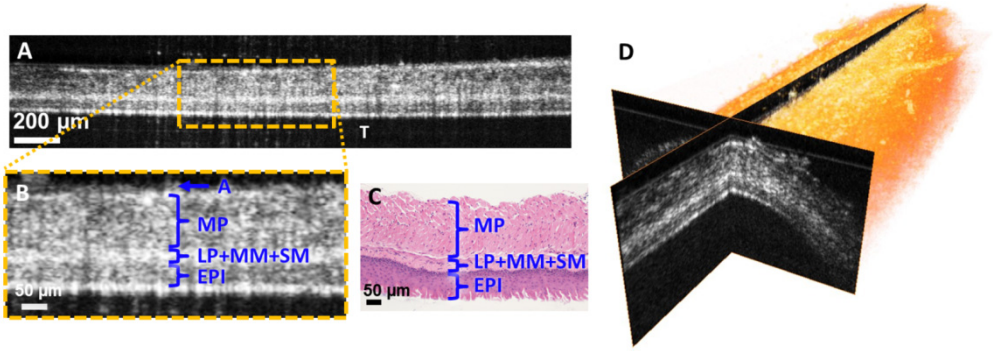

Fig. 2. OCT images of a normal esophagus obtained from a WT (*Tslpr*$^{+/+}$ control) mouse. OCT cross-sectional image (A) and its magnified view (B) showing different esophageal sub-layers (EPI-epithelium, LP-lamina propria, MM-muscularis mucosae, SM-sub-mucosa, MP-muscularis propria and A-adventitia; T-plastic tube). (C) Representative histology of normal esophagus of a WT healthy mouse. D) 3D rendering of an OCT volumetric data set (3x1.5x1.5 mm^3) obtained from the middle region of the esophagus (Media 1). T denotes the plastic tube.

OCT images acquired from the middle region of a normal, healthy (*Tslpr*$^{+/+}$ control) mouse are shown in Fig. 2. The epithelium (EPI) appeared as a low scattering layer in the OCT image. As seen in Figs. 2(B) and 2(C), the lamina propria (LP), muscularis mucosae (MM) and sub-mucosa (SM) are indistinct in the mouse esophagus, and appeared as a bright layer in the OCT cross-section. Muscularis propria (MP), which is composed predominantly of skeletal muscle, appeared as a thick low scattering layer that is surrounded by a thin layer of adventitia [Fig. 2(B)]. Figure 2(D) shows the 3D OCT rendering of the middle region of a healthy mouse esophagus (Media 1). Cut-through views showing the esophageal layers in two orthogonal directions depict the optical biopsy capabilities of OCT.

#201290 - $15.00 USD Received 14 Nov 2013; revised 17 Jan 2014; accepted 18 Jan 2014; published 27 Jan 2014

3.2 Esophagus of mice with EoE-like disease

To determine morphological features associated with murine EoE-like disease, OCT images obtained from the esophagus of *Tslpr*$^{+/+}$ control (WT healthy) and *Tslpr*$^{+/+}$ treatment mice (WT mice with EoE-like disease) were compared. As seen in Figs. 3(A) and 3(B), the layered architecture of the esophagus in *Tslpr*$^{+/+}$ treatment mice appeared similar to that of *Tslpr*$^{+/+}$ control mice. The average epithelial thickness in *Tslpr*$^{+/+}$ treatment mice (67.2 +/– 20.9 μm) was ~17% higher than that of *Tslpr*$^{+/+}$ control (57.5 +/– 9.6 μm) mice [Fig. 3(C)]. However, the thickness difference did not reach statistical significance with the sample size used in this study (n = 6 in *Tslpr*$^{+/+}$ control group and n = 9 in *Tslpr*$^{+/+}$ treatment group, p = 0.31), due to the large standard deviation in *Tslpr*$^{+/+}$ treatment mice group.

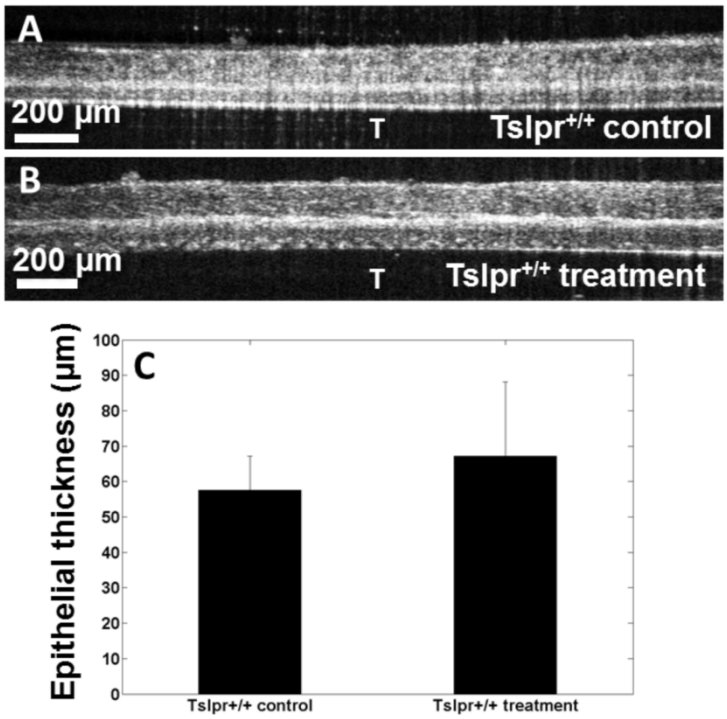

Fig. 3. Esophageal epithelial thickness in *Tslpr*$^{+/+}$ control (healthy) and *Tslpr*$^{+/+}$ treatment (mice with EoE-like disease) groups. OCT image from the esophagus of a *Tslpr*$^{+/+}$ control mouse (A) and a *Tslpr*$^{+/+}$ treatment mouse with EoE-like disease (B). C) Comparison of the epithelial thickness in *Tslpr*$^{+/+}$ control and *Tslpr*$^{+/+}$ treatment mice groups. T denotes the location of the inserted plastic tube.

Food impaction, a common symptom in EoE patients, is a sign of esophageal dysfunction [54, 55]. In this study, the incidence rate of food impaction in *Tslpr*$^{+/+}$ treatment mice group was ~30% [40]. The morphological features of the esophagus near the location of food impaction in *Tslpr*$^{+/+}$ treatment mice were visualized using OCT [Fig. 4 and Media 2]. Food impaction was present at multiple locations along the length of the esophagus (anterior, middle and posterior regions) in *Tslpr*$^{+/+}$ treatment mice. Figure 4(C) shows food impaction that occurred close to the esophageal-stomach junction of a *Tslpr*$^{+/+}$ treatment mouse.

3.3 Characterization of EoE-like disease in Tslpr$^{+/+}$ *and Tslpr*$^{-/-}$ *mice*

OCT was utilized to compare the morphological features of the esophagus in control and treatment groups of Tslpr$^{+/+}$ and Tslpr$^{-/-}$ mice. As shown in Fig. 5, the thickness variations of esophageal sub-layers in different mice groups could be determined from the OCT cross-

#201290 - $15.00 USD Received 14 Nov 2013; revised 17 Jan 2014; accepted 18 Jan 2014; published 27 Jan 2014

sectional images. The morphological features observed in the OCT images corresponded well with the representative histology sections from each mice group. Figures 5(C) and 5(D) show the epithelial thickening associated with esophageal inflammation in a Tslpr$^{+/+}$ treatment mouse. The reduction in thickness of the esophagus in a Tslpr$^{-/-}$ treatment mouse is shown in Figs. 5(G) and 5(H).

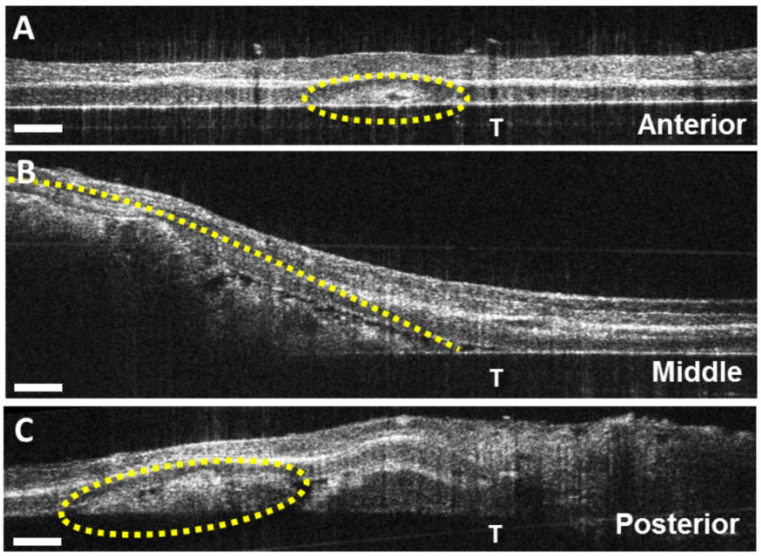

Fig. 4. Food impaction in Tslpr$^{+/+}$ treatment group (mice with EoE-like disease). (A-C) OCT cross-sectional images obtained from the food impaction sites that occurred at different regions of esophagus in Tslpr$^{+/+}$ treatment mice (Media 2). Yellow markings show trapped food particles. Scale bars denote 200 μm and T denotes the location of the inserted plastic tube.

The thickness of different esophageal layers was determined from the center region of the esophagus and compared in Fig. 6. Epithelial thickness was highest in *Tslpr*$^{+/+}$ treatment mice group (67.2 +/– 20.9 μm) and lowest in *Tslpr*$^{-/-}$ treatment mice group (41.4 +/– 4.7 μm, p = 0.01). The epithelial thickness in the *Tslpr*$^{+/+}$ mice groups (63.3 +/– 17.5 μm) was significantly higher than that in the *Tslpr*$^{-/-}$ mice groups (43.6 +/– 5.5 μm, p = 0.002). As observed in human EoE patients [56], the higher standard deviation of epithelial thickness in the *Tslpr*$^{+/+}$ treatment mice group may be due to the patchy nature of EoE-associated epithelial inflammation. LP + MM + SM thickness in the *Tslpr*$^{+/+}$ treatment group (37.4 +/– 4.9 μm) was significantly higher than that in the *Tslpr*$^{-/-}$ treatment group (32.2 +/– 2.5 μm, p = 0.03), but did not achieve significant difference compared to the *Tslpr*$^{-/-}$ control group (34.2 +/– 2.2 μm, p = 0.24). In general, the thickness of LP + MM + SM was higher in the *Tslpr*$^{+/+}$ mice group (37.9 +/– 4.2 μm) than that in the *Tslpr*$^{-/-}$ mice group (33.0 +/– 2.5 μm, p = 0.003).

The average muscle layer thickness in the *Tslpr*$^{-/-}$ treatment group (71.1 +/– 8.3 μm) was significantly lower than in the *Tslpr*$^{+/+}$ control (95.5 +/– 6.48 μm, p < 0.001) and *Tslpr*$^{-/-}$ control (93.6 +/– 12.7 μm, p = 0.009) groups. The MP thickness in the *Tslpr*$^{+/+}$ treatment group showed higher standard deviation (22.3 μm; n = 9), especially for those values obtained from regions close to food impaction sites. Interestingly, the muscle layer thickness of both mice treatment groups (81.0 +/– 19.4 μm) was lower in comparison to the control mice of either genotype (94.7 +/– 8.8 μm, p = 0.05). Since the differences in the EPI and MP thicknesses balanced out, the total thickness of the *Tslpr*$^{+/+}$ control (191.5 +/– 15.2 μm) and treatment (192.2 +/– 22.1 μm) groups were quite similar. Overall, the total thickness of the

#201290 - $15.00 USD Received 14 Nov 2013; revised 17 Jan 2014; accepted 18 Jan 2014; published 27 Jan 2014

esophagus in the *Tslpr*$^{+/+}$ mice groups (191.9 +/– 19.0 μm) was significantly higher than that in the *Tslpr*$^{-/-}$ mice groups (156.7 +/– 19.9 μm, $p < 0.001$). Another notable characteristic was that total thickness in the *Tslpr*$^{-/-}$ treatment mice group (144.7 +/– 12.7 μm) was significantly lower than all other groups. Thus, these results suggest that thickness of esophageal layers can vary significantly depending on the genotype and treatment conditions, and OCT is a promising label-free imaging technique that can be used to precisely characterize morphological changes in the esophagus.

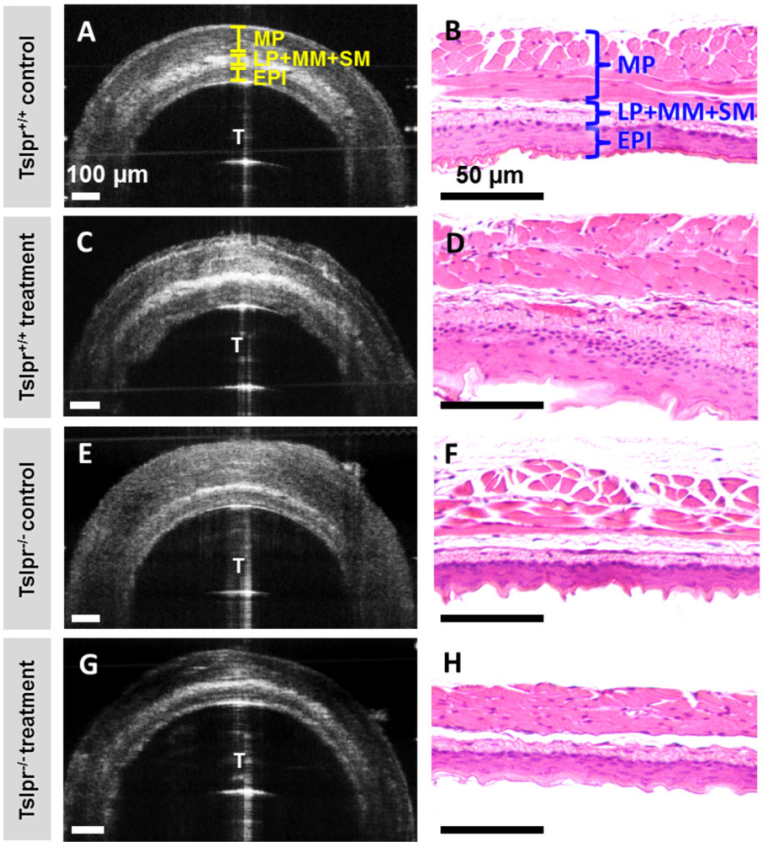

Fig. 5. Comparison of OCT images obtained from different mice groups and their representative histology. Representative OCT cross-section and histology obtained from (A, B) *Tslpr*$^{+/+}$ control, (C,D) *Tslpr*$^{+/+}$ treatment, (E, F) *Tslpr*$^{-/-}$ control and (G, H) *Tslpr*$^{-/-}$ treatment mice groups. Scale bars denote 100 μm in OCT images and 50 μm in histology. T denotes the location of the inserted plastic tube.

4. Discussion

The direct involvement of the TSLP pathway in the pathogenesis of murine EoE-like disease was investigated in this study using OCT by utilizing *Tslpr*$^{+/+}$ and *Tslpr*$^{-/-}$ mice. Because of the thin nature of mouse esophagus (<0.3 mm), the penetration depth of 1-2 mm offered by OCT was sufficient to visualize all esophageal layers. The increased epithelial thickness and food impaction observed in the *Tslpr*$^{+/+}$ treatment group sensitized with MC903 + OVA and challenged with OVA confirmed the involvement of TSLP in the development of murine EoE-like disease [40]. In addition, absence of similar symptoms in the *Tslpr*$^{-/-}$ treatment group sensitized with MC903 + OVA and challenged with OVA showed that the TSLP pathway is very critical for EoE pathogenesis. The thickness of the muscle layer was expected to be higher in the *Tslpr*$^{+/+}$ treatment group, potentially related to the increased incidence of

#201290 - $15.00 USD Received 14 Nov 2013; revised 17 Jan 2014; accepted 18 Jan 2014; published 27 Jan 2014

food impaction in these animals. In contrast, MP layer thickness in both *Tslpr*$^{+/+}$ and *Tslpr*$^{-/-}$ treatment groups was lower than in the *Tslpr*$^{+/+}$ and *Tslpr*$^{-/-}$ control groups. These data indicate the effect of MC903 + OVA sensitization followed by OVA challenge on the esophageal muscle layer. Similarly, the total thickness of the esophagus was significantly lower in the *Tslpr*$^{-/-}$ treatment group, which shows the combined effect of TSLP mutation and MC903 sensitization on esophageal thickness. However, more studies are needed to determine the associated pathways and mechanisms leading to thickness variations in esophageal sub-layers.

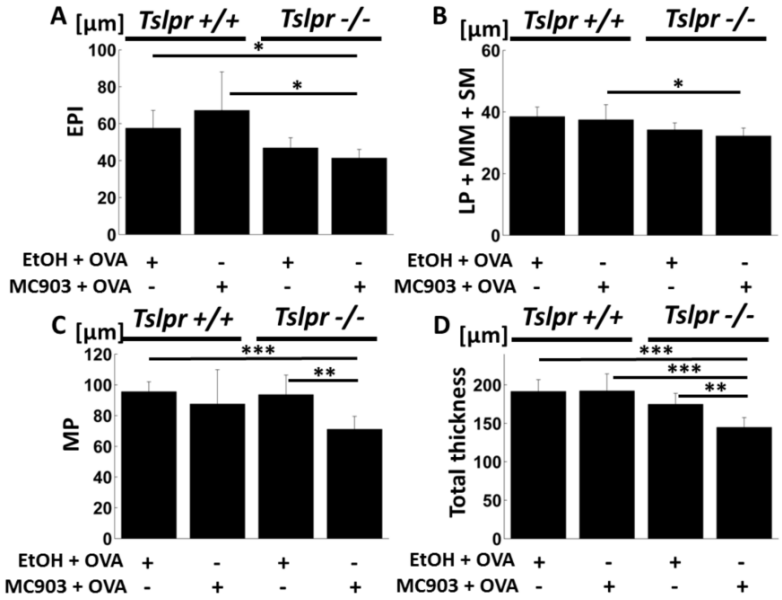

Fig. 6. Analysis of esophageal layer thickness in *Tslpr*$^{+/+}$ control, *Tslpr*$^{+/+}$ treatment, *Tslpr*$^{-/-}$ control and *Tslpr*$^{-/-}$ treatment mice groups. Comparison of thickness of A) EPI, B) LP + MM + SM, C) MP and D) Total esophageal thickness. (*, $p \leq 0.05$; **, $p \leq 0.01$; ***, $p \leq 0.001$).

The most challenging aspects of EoE diagnosis are the similarities of its symptoms with those of other upper GI disorders such as gastroesophageal reflux disease, and the unknown pathophysiological mechanisms underlying the development of EoE [5]. Hence, identification of EoE-associated immunological pathways and effective diagnostic markers of EoE is extremely important. As a label-free scattering contrast-based optical imaging technique that can provide spatial resolutions comparable to histology, OCT is emerging as a promising tool for detecting GI disorders [20, 22, 57]. Due to the variability in EoE diagnostic criteria [58] and the patchy nature of EoE-associated inflammation [56], the additional micro-structural 3D information obtained using a non-invasive *in vivo* imaging technique such as OCT can be critical in making the correct diagnosis. However, it is necessary to identify the pathological changes associated with EoE that can be visualized using OCT. In this study, the capability of OCT to characterize esophageal tissues in the context of mice with EoE-like disease and thus to assist in understanding the underlying pathophysiological mechanisms of this disease has been demonstrated. All the layers of mouse esophagus were visualized and the thickness of each layer was precisely determined using OCT. Even though thicker than mouse esophagus, thickness of EPI and LP / MM layers of human esophagus can be quantified using OCT [20, 22]. Unlike histology, the esophageal layer thickness values obtained using OCT are free from fixation and processing artifacts. As seen in the representative histology sections in Fig. 5, the esophageal layers appeared to be constricted after histological processing of paraformaldehyde-fixed tissue.

#201290 - $15.00 USD Received 14 Nov 2013; revised 17 Jan 2014; accepted 18 Jan 2014; published 27 Jan 2014

One of the limitations of OCT in characterizing small-animal disease models is its limited structural contrast. The effectiveness of OCT can be further enhanced by using multimodal imaging approaches. The anatomical scattering contrast provided by OCT will be complemented by molecular/biochemical contrast provided by complementary imaging techniques. In pre-clinical studies using mouse cancer models, dual-modality instruments employing OCT and fluorescence microscopy were shown to be capable of extracting micro-structural and molecular information from tumor regions [59, 60]. The complementary information obtained through multimodal OCT imaging can be helpful in pre-clinical research to understand underlying molecular mechanisms, to identify appropriate structural/molecular biomarkers for specific diseases and to monitor therapeutic interventions.

In this *ex vivo* study, it was possible to obtain OCT images by illuminating the probe beam on the esophageal specimen from its periphery. However, it is desirable to acquire *in vivo* images of the mouse esophagus using catheter-based or endoscopic probes. Due to the narrow lumen of the murine esophagus, extremely thin imaging probes are needed for obtaining *in vivo* images. OCT images of murine esophagus can be recorded *in vivo* using 0.9 mm external diameter catheters containing an OCT ImageWire (St. Jude Medical Inc., St. Paul, Minnesota, USA), which is widely used in cardiovascular OCT for imaging coronary arteries and deployed stents [61, 62]. Moreover, miniature endoscopes capable of providing high quality OCT images have been designed and developed using lens-free large core fibers (360 μm probe) [63]. Using these miniature probes, OCT permits *in vivo* and longitudinal studies in murine GI disease models, which can provide critical information related to pathogenesis, disease progression and treatment effects. Furthermore, endoscopic OCT has been successfully used in clinical GI studies for tissue differentiation [64], tumor staging [65] and treatment monitoring [25]. Endoscopic OCT can also be used in EoE patients to further our understanding of EoE pathogenesis and disease progression.

5. Conclusions

OCT was capable of differentiating esophageal sub-layers and monitoring structural changes in a murine model of EoE-like disease. Mice with EoE-like disease could be differentiated from control mice based on epithelial thickening and a higher incidence of food impaction. Regardless of the genotype, the muscle layer thickness appeared to be influenced by the treatment condition. The TSLP pathway was determined to be an important factor in mediating the thickness of esophageal sub-layers in the context of murine EoE-like disease by examining the esophagus of $Tslpr^{+/+}$ and $Tslpr^{-/-}$ mice under control and treatment conditions. The potential of OCT to act as a high-resolution label-free imaging tool to characterize murine models with EoE-like disease and thus to identify functional pathways associated with EoE pathogenesis was demonstrated.

Acknowledgments

This work was supported by the Lehigh University Start-up Fund and the National Institute of Health / National Institute of Biomedical Imaging and Bioengineering (NIH/NIBIB) Pathway to Independence Award (R00-EB010071 to C. Z.). Research in the Artis lab is supported by the US National Institutes of Health (AI061570, AI087990, AI074878, AI095776, AI102942, AI095466, AI095608, and AI097333 to D.A.), the Swiss National Science Foundation Prospective and Advanced Research Fellowships (PBBEP3_130438 and PA00P3_136468 to M.N.), T32-AI060516 and F32-AI098365 to E.D.T.W., and the Burroughs Wellcome Fund Investigator in Pathogenesis of Infectious Disease Award to D.A. This work was supported by the US National Institutes of Health/US National Institute of Diabetes and Digestive and Kidney Diseases P30 Center for Molecular Studies in Digestive and Liver Diseases (P30-DK050306), its pilot grant program and scientific core facilities (Molecular Pathology and Imaging, Molecular Biology, Cell Culture and Mouse), as well as the Joint Children's Hospital of Philadelphia-Penn Center in Digestive, Liver and Pancreatic Medicine and its pilot grant program. We also thank the Matthew J. Ryan Veterinary Hospital Pathology Lab, University of Pennsylvania, Philadelphia, USA.